JOURNAL OF VIROLOGY, May 2006, p. 4878–4889 Vol. 80, No. 10
0022-538X/06/$08.00+0 doi:10.1128/JVI.80.10.4878–4889.2006

N-Glycans on Nipah Virus Fusion Protein Protect against Neutralization but Reduce Membrane Fusion and Viral Entry

Hector C. Aguilar,[1] Kenneth A. Matreyek,[1] Claire Marie Filone,[2] Sara T. Hashimi,[1] Ernest L. Levroney,[1] Oscar A. Negrete,[1] Andrea Bertolotti-Ciarlet,[2] Daniel Y. Choi,[1] Ian McHardy,[1] Jennifer A. Fulcher,[3] Stephen V. Su,[1] Mike C. Wolf,[1] Luciana Kohatsu,[3] Linda G. Baum,[3] and Benhur Lee[1,3,4]*

Department of Microbiology, Immunology and Molecular Genetics,[1] Department of Pathology and Laboratory Medicine,[3] and AIDS Institute,[4] David Geffen School of Medicine at UCLA, Los Angeles, California 90095, and Department of Microbiology, University of Pennsylvania, Philadelphia, Pennsylvania 19104[2]

Received 19 December 2005/Accepted 28 February 2006

Nipah virus (NiV) is a deadly emerging paramyxovirus. The NiV attachment (NiV-G) and fusion (NiV-F) envelope glycoproteins mediate both syncytium formation and viral entry. Specific N-glycans on paramyxovirus fusion proteins are generally required for proper conformational integrity and biological function. However, removal of individual N-glycans on NiV-F had little negative effect on processing or fusogenicity and has even resulted in slightly increased fusogenicity. Here, we report that in both syncytium formation and viral entry assays, removal of multiple N-glycans on NiV-F resulted in marked increases in fusogenicity (>5-fold) but also resulted in increased sensitivity to neutralization by NiV-F-specific antisera. The mechanism underlying the hyperfusogenicity of these NiV-F N-glycan mutants is likely due to more-robust six-helix bundle formation, as these mutants showed increased fusion kinetics and were more resistant to neutralization by a fusion-inhibitory reagent based on the C-terminal heptad repeat region of NiV-F. Finally, we demonstrate that the fusogenicities of the NiV-F N-glycan mutants were inversely correlated with the relative avidities of NiV-F's interactions with NiV-G, providing support for the attachment protein "displacement" model of paramyxovirus fusion. Our results indicate that N-glycans on NiV-F protect NiV from antibody neutralization, suggest that this "shielding" role comes together with limiting cell-cell fusion and viral entry efficiencies, and point to the mechanisms underlying the hyperfusogenicity of these N-glycan mutants. These features underscore the varied roles that N-glycans on NiV-F play in the pathobiology of NiV entry but also shed light on the general mechanisms of paramyxovirus fusion with host cells.

Nipah virus (NiV) and Hendra virus (HeV) are emerging zoonotic viruses classified as members of a new *Henipavirus* genus within the *Paramyxoviridae* family (41). NiV and HeV are currently the only paramyxoviruses that are classified as biosafety level 4 pathogens. NiV infection involves respiratory and neurological sequelae, often resulting in fatal encephalitis, the primary cause of death in humans (14, 39). In 1999 to 2000, NiV outbreaks among agricultural workers in Malaysia and Singapore resulted in a 40% mortality rate, primarily from fatal encephalitis, as well as destruction of livestock worth over $100 million (14). More recent NiV outbreaks in Bangladesh had mortality rates approaching that seen for Ebola virus (up to 74%) (44, 46), underscoring the need for therapeutic and vaccine development against this pathogen.

Endothelial syncytium formation is a peculiar hallmark of NiV infection (45) and results in endothelial cell destruction, inflammation, and hemorrhage. Both the fusion (F) and attachment (G) envelope glycoproteins in NiV and HeV are necessary for viral entry, cell-cell fusion, and syncytium formation. We and others recently found that NiV and HeV use the same receptor, ephrinB2, for cellular entry, and the high level of expression of ephrinB2 on endothelial cells and neurons largely accounts for the cellular tropism of NiV and HeV (4, 25). Interestingly, galectin 1, an endogenous lectin secreted by endothelial cells, can bind to specific N-glycans on NiV-F and inhibit NiV envelope-mediated cell-cell fusion (17), suggesting that N-glycans on the viral envelope glycoprotein play a critical role in the pathobiology of NiV entry into host cells.

N-glycans on viral envelope glycoproteins serve many functions, such as promoting efficient expression and transport, facilitating fusion, binding to cell surface receptors, and protecting against neutralization by antibodies. For example, glycosylation of viral envelope glycoproteins of human immunodeficiency virus (HIV) and influenza, West Nile, Ebola, and Newcastle disease viruses affects fusogenicity of the envelope glycoproteins and viral infectivity (26, 40, 42) and direct interaction of N-glycans on the dengue virus envelope protein with the C-type lectin DC-SIGN facilitates its entry (24). Envelope-associated N-glycans also play a role in "shielding" the virus against antibody neutralization, as observed for HIV, simian immunodeficiency virus (SIV) (8, 27, 42), equine infectious anemia virus (EIAV) (33), hepatitis B virus (HepB) (16), and influenza virus (37) (reviewed in reference 27), although a similar role for N-glycans in paramyxovirus envelope proteins has yet to be reported.

Both NiV-F and HeV-F are heavily glycosylated (7, 17, 21), and it is likely that the N-glycans on NiV-F and HeV-F play critical

* Corresponding author. Mailing address: Department of MIMG, 3825 MSB, 609 Charles E. Young Drive East, UCLA, Los Angeles, CA 90095. Phone: (310) 206-8792. Fax: (310) 267-2580. E-mail: bleebhL@ucla.edu.

roles in their biological function, as has been shown for N-glycans on the fusion proteins of other paramyxoviruses (3, 40). However, the fusogenicities of NiV-F and HeV-F appear unusually resistant to the effects of N-glycan removal. Thus, while removal of specific N-glycans on other paramyxoviruses has resulted in severe defects in folding, transport, and fusion activity (3, 40), removal of individual glycans in NiV-F and HeV-F appears to have little negative effect on fusogenicity. Indeed, the removal of specific N-glycans on NiV-F and HeV-F resulted in slightly increased cell-cell fusion efficiencies (7, 21).

Here, we examine the mechanisms underlying the hyperfusogenic phenotype caused by removal of specific N-glycans on NiV-F and highlight the varied roles that N-glycans on NiV-F play in the pathobiology of NiV entry.

MATERIALS AND METHODS

NiV codon optimization and expression plasmids. The codon-optimized NiV-F and NiV-G gene products were tagged at their C termini with the AU1 or hemagglutinin tag, respectively, as previously described (17). NiV-HR2-Fc and HIV-HR2-Fc were constructed by fusing the sequence of the heptad repeat region 2 of NiV-F (amino acids 447 to 488) or of HIV-1 gp41 (T20 peptide sequence) (43) with the Fc constant region of human immunoglobulin G1 (IgG1) (25), respectively.

Cell culture. 293T, MDCK, HeLa, and PK13 cells were grown in Dulbecco's modified Eagle's medium containing 10% fetal bovine serum (FBS). Vero cells were grown in minimal essential medium alpha, containing 10% FBS. 293T and Vero cells were obtained from the ATCC. PK13 cells (porcine fibroblasts) were a kind gift from Irvin Chen at UCLA School of Medicine, Los Angeles, CA.

Quantitation of cell-cell fusion. Wild-type (WT) or mutant NiV-F and NiV-G expression plasmids (1:1 ratio, 1 μg total) were transfected with or without pcDNA3.1 as filler DNA into 293T or Vero cells growing in 12-well plates at 80% confluence. At 12 to 18 h posttransfection, cells were stained with DAPI (4′,6′-diamidino-2-phenylindole), and syncytium formation was quantified by counting the number of nuclei in syncytia per 100× field (at least 10 fields were counted per condition). Syncytia are defined as four or more nuclei visualized within a common cell membrane.

Production of anti-NiV-F and anti NiV-G antisera and quantification of NiV-F and NiV-G cell surface expression (CSE) levels. Production of antisera from genetically immunized rabbits (using NiV-M and -F or -G expression plasmids) was previously described (25). Sera containing anti-F- or anti-G-specific activities were used for flow cytometry on NiV-F/G-transfected cells at a 1:1,000 dilution. Bound antibody was detected with phycoerythrin-conjugated goat anti-rabbit antibodies (Caltag, Burlingame, CA). Antisera were also raised in rabbits immunized with peptides corresponding to amino acids 39 to 57 and 331 to 348 of NiV-F_2 and NiV-G, respectively. These regions were previously shown to be immunogenic (6).

Quantitation of viral entry and viral genome copies. NiV-F and -G were pseudotyped onto a reporter vesicular stomatitis virus (VSV) as described previously (25). For a more rapid and accurate quantitation of viral entry, the *Renilla* luciferase reporter gene was cloned in place of the red fluorescence protein reporter gene. Vero cells plated in 48-well plates were infected with pseudotyped virions in phosphate-buffered saline (PBS) plus 1% FBS for 2 h at 37°C over a 6-log viral dilution span (10^{-1} to 10^{-6}). After 2 h, cells were washed, and Vero cell growth medium was added. At 24 h postinfection, cells were lysed, and luciferase activity was measured as relative light units (RLU) using a *Renilla* luciferase detection system (Promega, Madison, WI) and a Veritas microplate luminometer (Turner Biosystems, Sunnyvale, CA). For the quantitation of viral genome copies, viral RNA extracted from the viral preparations using an RNA extraction kit (QIAGEN, Valencia, CA) was used for a reverse transcriptase reaction using an iScript cDNA synthesis kit (Bio-Rad, Hercules, CA). The number of VSV genomes was then quantified using quantitative PCR according to a protocol which can quantify the number of VSV genomes from cell culture material (29). This assay uses primers and probes targeted to the L gene of the Indiana serotype, the parental virus from which the reporter vector was derived. Real-time PCR was performed on a DNA Engine Opticon 2 multiplexing real-time PCR machine (MJ Research).

Analysis of total cell or surface NiV-F and -G proteins. NiV-F and/or NiV-G expression plasmids were transfected into 293T cells plated in six-well plates (2 μg of plasmid/well). Cells were either cell surface biotinylated or not, as indicated. Biotinylated proteins were precipitated using streptavidin-agarose beads (Pierce). Twenty percent of total cell lysate or precipitated biotinylated proteins was loaded onto a sodium dodecyl sulfate-polyacrylamide gel and subsequently detected by Western blotting using the antitag, anti-F_2, or anti-G peptide antibodies, as indicated. Primary and secondary antibodies were used at 1:1,000 and 1:20,000 dilutions, respectively, followed by ECL Plus detection (Amersham Biosciences, Piscataway, NJ).

Production of NiV-HR2-Fc and HIV-HR2-Fc immunoadhesins and fusion inhibition. NiV-HR2-Fc, HIV-HR2-Fc, or Fc-only expression plasmids were transfected into 293T cells, and 24 h posttransfection supernatants were collected and concentrated using a Centriplus filter YM-10 concentrator (Millipore, Bedford, MA). Protein concentrations were measured by an Fc-specific enzyme-linked immunosorbent assay as previously described (25). For NiV fusion inhibition, the indicated amounts of NiV-HR2-Fc or HIV-HR2-Fc were added to 293T or Vero cells transfected with NiV-G and WT or N-glycan mutant NiV-F expression plasmids. Fusion was quantified after overnight incubation as described above. HIV type 1 (HIV-1) entry inhibition was measured as previously described by Derdeyn et al., except that the NiV-HR2-Fc or HIV-HR2-Fc protein were used instead of T20 (9).

Fusion kinetics of WT or mutant NiV-F proteins. The fusion kinetics of WT and mutant NiV-F proteins were determined in a β-lactamase reporter cell-cell fusion assay, as previously described (18, 31). Fusion-nonpermissive PK13 effector cells were cotransfected with β-lactamase, NiV-G, and WT or mutant NiV-F expression constructs using Lipofectamine 2000. These were then added to 293T target cells labeled with CCF2-AM dye. Effector and target cells were mixed and incubated at 37°C, and cell-cell fusion was detected by analyzing the shift from green to blue fluorescence, indicating β-lactamase cleavage of CCF2. Fluorescence was quantified every 3 min using a CytoFluor Series 4000 fluorescence multiwell plate reader (PerSeptive Biosystems, Framingham, MA). The results are expressed as the ratio of blue to green fluorescence obtained with NiV-G- and NiV-F-transfected effectors minus the background blue and green fluorescence obtained with empty-vector-transfected cells.

NiV-F/NiV-G coimmunoprecipitation. 293T cells in 10-cm plates were transfected with 20 μg of the indicated NiV-F/G plasmids at a 1:1 ratio using Lipofectamine 2000. At 24 h posttransfection, cells were lysed, and cell lysates were subjected to immunoprecipitation as previously described (17), using a 1:100 dilution of anti-NiV-G or anti-NiV-F antisera, as indicated, in immunoprecipitation buffer (PBS, 1% Triton X-100, 0.1% sodium dodecyl sulfate, 0.5% sodium deoxycholate, 1× complete protease inhibitor mix [Roche, Indianapolis, IN]) and protein G agarose beads (Pierce, Rockford, IL). Beads were washed five times with wash buffer (PBS, 2 mM EDTA, 0.2% NP-40). Coimmunoprecipitated (co-IP) proteins were analyzed by Western blotting as described above using antitag antibody and quantified by densitometry using a VersaDoc Imaging System (Bio-Rad, Hercules, CA).

Modeling of paramyxovirus F protein structures. The known structure most homologous to NiV-F is the human parainfluenza virus type 3 (HPIV-3) F protein. The HPIV-3 F sequence identity to NiV-F is 28%. In cases of sequence homologies lower than 30%, threading methods are able to yield more accurate results than other methods, since in these methods structural information is used to compare an amino acid sequence to a library of known folds (34). The Phyre threading program (http://www.sbg.bio.ic.ac.uk/~phyre/) revealed HPIV-3 F template structure (Protein Data Bank code 1ztm) as the best template structure. Threading through this template structure received an E-value score of 0, which by programmatic criteria suggests a high level of confidence in the predicted structure. The same threading algorithm was run on all the other paramyxovirus F proteins; HPIV-3 was the best template structure for all, with the exception of Newcastle disease virus (NDV) and simian virus 5 (SV5), where it was the second best. Results for sequence identity were 27% for Hendra virus, 26% for canine distemper virus (CDV), 28% for phocine distemper virus (PDV), 27% for pestes-des-petits-ruminants virus (PPRV), 28% for rinderpest virus (RPV), 44% for Sendai virus (SeV), 44% for HPIV-1, 25% for SV5, and 26% for NDV. All modeled F proteins had E-values of 0, with the exception of RPV, which had an E-value of $1.6e^{-42}$. The structural coordinates generated by our modeling were visualized using Rasmol version 2.7.2.1. N-linked glycosylation sites of each F protein were also visualized in Rasmol.

Protein structure accession numbers. Protein accession numbers are as follows: NiV, NP_112026.1; HeV, NP_047111.2; measles virus (MeV), AAB26145.1; RPV, CAA83481.1; PPRV, CAJ01699.1; CDV, AAD18007.1; PDV, BAA01206.1; SeV, AAB06830.1; HPIV-1, BAA04154.1; HPIV-3, AAB21447.1; SV5, BAA85590.1; and NDV, CAA50869.1.

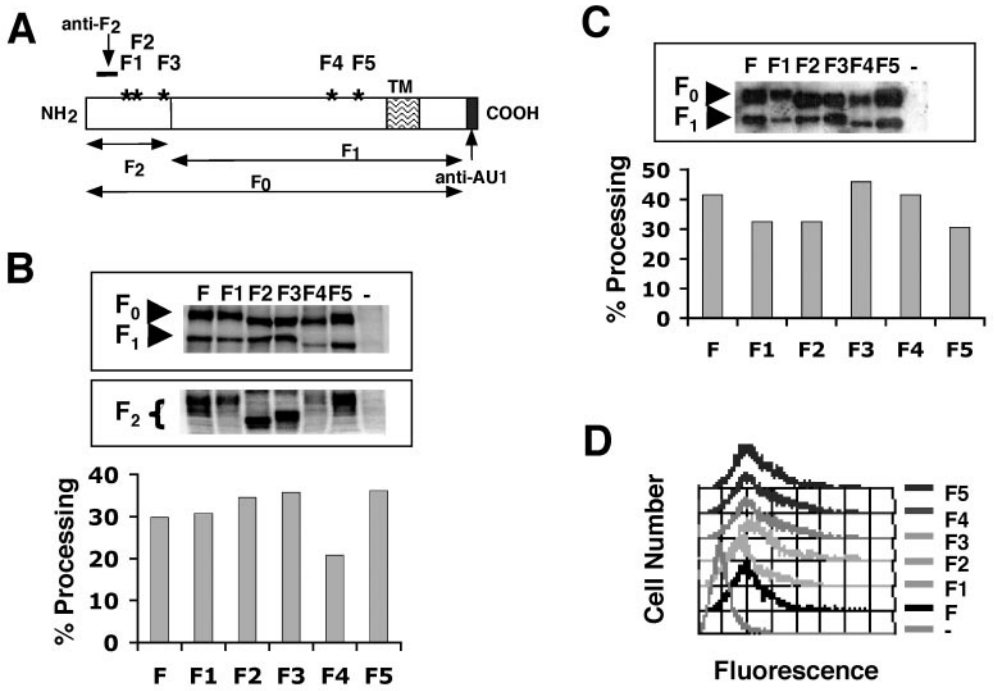

FIG. 1. Analysis of NiV-F N-glycan site utilization. (A) Schematic of NiV-F glycoprotein. NiV-F (F_0) is a type I transmembrane protein that is cleaved into F_1 and F_2 by a host cell protease. Asterisks represent potential N-linked glycosylation sites F1 to F5. The epitope of NiV-F_2 antipeptide antibody is indicated. Codon-optimized NiV-F was AU1 epitope tagged at the C terminus as indicated. (B) Top: analysis of immunoprecipitated WT and mutant NiV-F proteins (F, F1, F2, F3, F4, and F5). Briefly, ^{35}S-radiolabeled cell lysates were cleared out using goat anti-rabbit IgG at a 1:100 dilution, and supernatants were immunoprecipitated using a 1:100 combination of polyclonal anti-NiV-F antisera (25) and the anti-F_2 peptide antisera described above (A) at a 1:1 ratio. Relative mobilities of the precursor (F_0) and cleaved proteins (F_1 and F_2) showed usage of F2, F3, F4, and F5 glycosylation sites. Bottom: estimation of the relative levels of processing between the various single N-glycan mutant fusion proteins. Percent processing was calculated as the percentage of the sum of F_1 plus F_2 protein subunits divided by the total sum of NiV-F protein precursor and subunits ($F_0 + F_1 + F_2$), using phosphorimager quantitation of ^{35}S-radiolabeled protein subunits. One out of two representative experiments is shown. (C) Top: Western blot analysis of biotinylated cell surface proteins. Briefly, biotinylated 293T cells were precipitated with streptavidin-agarose beads and detected with a mouse anti-AU1 monoclonal antibody against AU1-tagged NiV-F. Percent processing was calculated as the percentage of F_1 subunits over the total sum of NiV-F protein precursor and the F_1 subunits ($F_0 + F_1$). One out of two representative experiments is shown. (D) Relative CSE of WT and mutant NiV-F proteins in 293T cells transfected with NiV-G and WT or N-glycan mutant NiV-F expression plasmids at a 1:1 ratio, using an anti-NiV-F-specific antiserum. Negative control (−) corresponds to cells expressing NiV-G only. Data shown are from one representative experiment out of four.

RESULTS

NiV-F is glycosylated on four of its five potential N-linked glycosylation sites. There are five potential N-linked glycosylation sites in NiV-F; the first three (F1, F2, and F3) are in the F_2 subunit and the last two (F4 and F5) are in the transmembrane F_1 subunit (Fig. 1A) (21). To examine if these sites were actually glycosylated, we made a conservative asparagine-to-glutamine change (N to Q) in position 1 of the glycosylation sequon $N^1X^2(S/T)^3$ (mutants F1, F2, F3, F4, and F5) (Fig. 1A) and examined the expression and mobilities of the sites in a radioimmunoprecipitation assay. Radiolabeled cell lysates from 293T cells expressing WT NiV-F or the F1 to F5 N-glycan mutants were immunoprecipitated and analyzed on a 10% or 14% polyacrylamide gel to effectively visualize the relative mobilities of the F_0/F_1 bands or the F_2 band, respectively. The F_1 band of the F4 and F5 mutants and the F_2 band of the F2 and F3 mutants migrated faster than the comparable bands of the WT NiV-F protein, indicating that these N-glycan sites were indeed glycosylated (Fig. 1B). The slightly faster migration exhibited by the F_0 band of the F2 to F5 mutants is consistent with this analysis. The F_0/F_1 and F_2 bands of the F1 mutant migrated equivalently with that of WT NiV-F, which suggests that the F1 site is not glycosylated. Thus, our results showing that the F2 to F5 sites are glycosylated in 293T cells are in agreement with results from the work of Moll et al. (21) obtained in MDCK cells.

Phosphorimaging analysis of F_0 processing into F_1 and F_2 subunits indicated that all five NiV-F N-glycan site mutants, with the possible exception of the F4 mutant, were processed about as efficiently as WT NiV-F (Fig. 1B) and were expressed at levels similar to or slightly lower than (for F1 and F4) those of the WT NiV-F protein (Fig. 1B, top). The heterogeneity in glycosylation for the F_2 band is more apparent than that of the F_0 or F_1 band due to its relatively lower molecular weight. Next, we biotinylated the cell surface of 293T cells expressing WT NiV-F or the indicated N-glycan mutants and assessed the levels of processing and expression of cell surface NiV-F by streptavidin immunoprecipitation followed by Western blot analysis (Fig. 1C). At the cell surface, all five mutant proteins were processed at levels comparable to those of the WT NiV-F protein (Fig. 1C), and their levels of expression were either

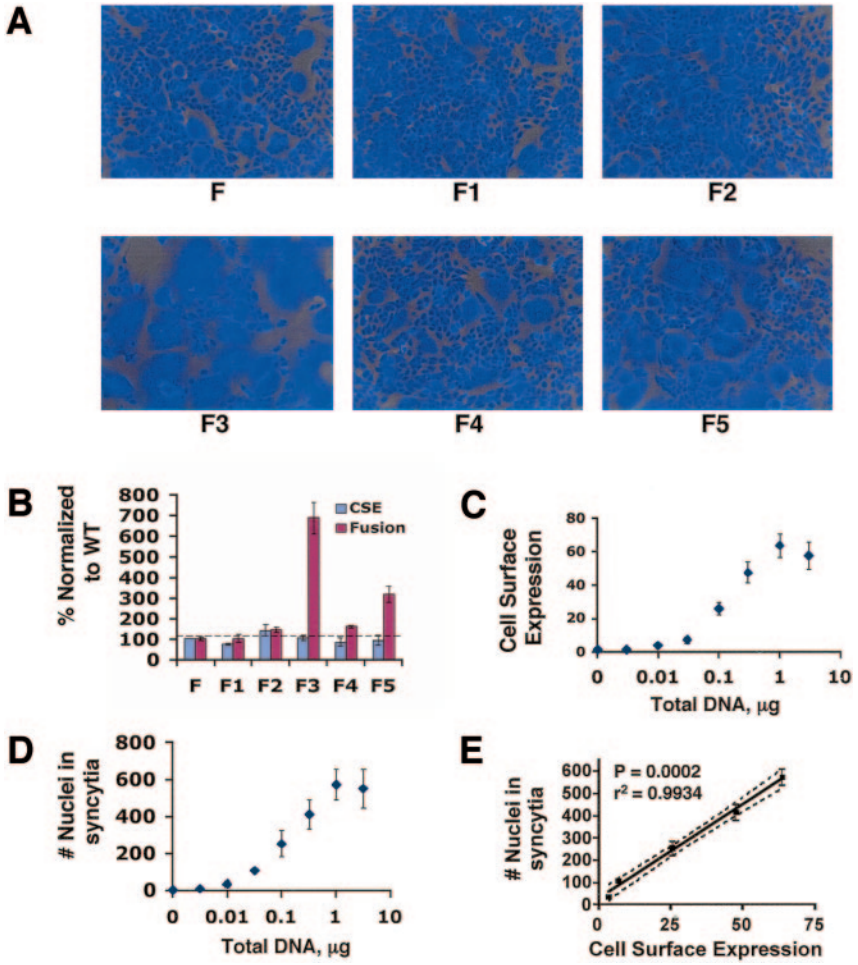

FIG. 2. The role of N-glycans on NiV-F in syncytium formation. (A) NiV-F (or the indicated N-glycan mutants) and NiV-G plasmids were transfected at a 1:1 ratio with Lipofectamine 2000 (0.3 μg NiV-F and -G/12-well plate). Cells were DAPI stained 18 h posttransfection, and representative images of syncytia formed are shown as DAPI images overlaid onto bright-field images. DAPI-stained nuclei appear blue, and syncytia appear as large clusters of blue nuclei surrounded by relatively clear cytoplasm. Syncytia are particularly evident in the F3 panel. (B) Relative levels of fusion and CSE obtained for WT NiV-F or single N-glycan mutant proteins in 293T cells. CSE was determined by flow cytometry as in Fig. 1D. Both fusion and CSE levels were separately normalized to levels seen for WT NiV-F protein, which were set at 100%. Data shown are averages ± standard errors from three independent experiments. (C) Titration of transfected NiV-F/G plasmids with the degree of CSE observed. The indicated amounts of NiV-F/NiV-G expression plasmids were cotransfected at a 1:1 ratio, and the total DNA amount transfected was kept constant with pcDNA3.1. Data for 293T cells are shown as averages ± standard deviations. One representative experiment out of three is shown. (D) Titration of transfected NiV-F/G plasmids with the degree of cell-cell fusion observed. The indicated amounts of NiV-F/NiV-G expression plasmids were cotransfected at a 1:1 ratio, and the total DNA amount transfected was kept constant with pcDNA3.1. Fusion was quantified in 293T and Vero cells as described in Materials and Methods. Data for 293T cells are shown as averages ± standard deviations from three independent experiments. One representative experiment out of three is shown. (E) The measure of cell-cell fusion from panel D was plotted against CSE from panel C. Pearson correlation analysis was performed using GraphPad PRISM.

similar to or slightly lower than (for F1 and F4) those of the WT NiV-F protein (Fig. 1C, top). Finally, in agreement with the analysis of surface proteins by biotinylation in Fig. 3C, the F1 to F5 N-glycan mutants had surface expression similar to that of WT NiV-F, as monitored by binding to a rabbit polyclonal anti-NiV-F-specific antiserum. A small decrease in the levels of surface expression was detected for the F1 and, to a lesser extent, the F4 mutant proteins (the latter not noticeable in this particular experiment) (compare Fig. 1D and Fig. 2B).

Removal of certain N-glycans on NiV-F results in increased fusogenicity. Having established that removal of N-glycans had little effect on F_0 processing or cell surface expression, we assessed whether removal of particular N-glycans had any effects on the fusogenicity of NiV-F. We transfected WT NiV-G and NiV-F or the F1 to F5 N-glycan mutants into permissive 293T cells and quantified the number of syncytia formed after 18 h. Since all the N-glycan mutants were expressed at levels similar to those of WT NiV-F, fusogenicity (for each of the N-glycan mutants) was normalized to the number of syncytia formed with WT NiV-F. Strikingly, the F3 and F5 N-glycan mutants exhibited fusion levels seven- and threefold higher than those of WT NiV-F (Fig. 2B), respectively. Representative images of syncytium formation exhibited by WT NiV-F and the F1 to F5 N-glycan mutants are shown in Fig. 2A. Similar but less marked differences were seen in Vero and MDCK cells (data not shown). In 293T cells, we found that the

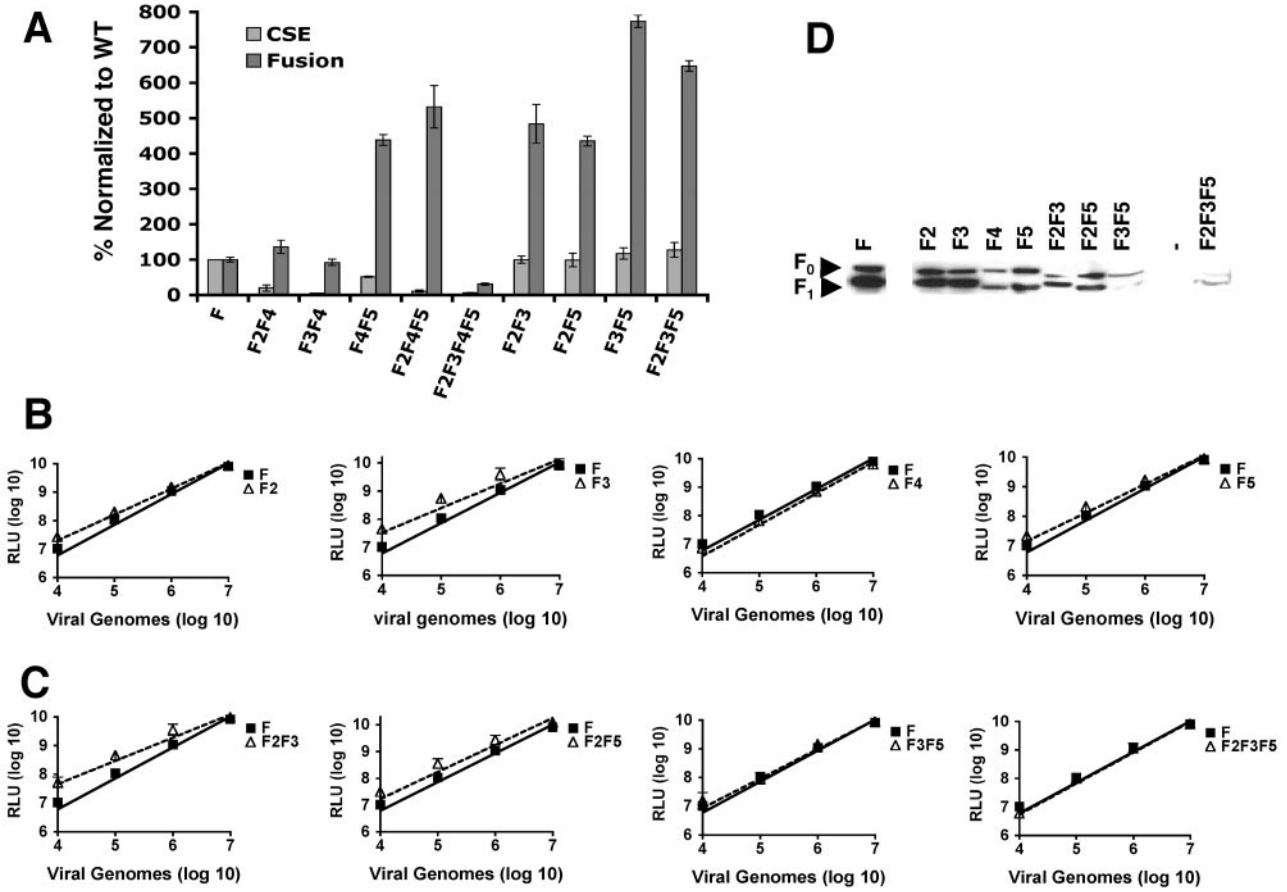

FIG. 3. Multiple N-glycans in combination on NiV-F inhibit cell-cell fusion and viral entry. (A) Relative levels of fusion versus CSE for WT NiV-F and multiple N-glycan mutants in 293T cells. Data are presented as values normalized to that of WT NiV-F (set at 100%) and are shown as averages ± standard errors from three separate experiments. (B and C) Relative entry levels of NiV-F/G-pseudotyped VSV-*Renilla*-luciferase reporter viruses (VSV-rluc). NiV-G and the indicated WT or mutant NiV-F proteins were pseudotyped onto luciferase reporter viruses as described in Materials and Methods. RLU were quantified 24 h postinfection and plotted against the number of viral genomes per ml. Relative amounts of genome copies in the viral preparations were analyzed by reverse transcription-PCR as described in Materials and Methods. Data shown are averages ± standard deviations from three independent experiments. Sometimes the error bars are not visible because they are too small to be seen in a logarithmic scale. (D) Western blot analysis of WT or mutant NiV-F proteins contained in viral preparations used in panels B and C and blotted with a mouse anti-AU1 monoclonal antibody, as described in Materials and Methods, showing F_0 and F_1 subunits. One representative experiment out of three is shown.

level of CSE (Fig. 2C) or cell-cell fusion (Fig. 2D) directly correlated with the amount of plasmid DNA transfected but that above a certain level (1 μg/12-well plate), a plateau was observed (Fig. 2C and D, respectively). Indeed, we were able to determine the range of DNA to be used that resulted in a linear relationship between cell surface expression and syncytium formation (Fig. 2E). Thus, in this and all other cell-cell fusion experiments, a DNA amount corresponding to the linear part of the dose response curve in Fig. 2C and D (0.3 μg/12-well plate) was used. In summary, these results indicate that removal of the F3 and F5 N-glycans increased the fusogenicity of NiV-F. This effect was most marked in 293T cells and was not due to differences in the CSEs of NiV-F or the efficiencies of F_0 processing.

Additive or synergistic effects of multiple N-glycans on reducing NiV-F-mediated fusion. Next, we made all possible double N-glycan site mutants (F2F3, F2F4, F2F5, F3F4, F3F5, and F4F5), selected triple mutants (F2F4F5 and F2F3F5), and the one quadruple mutant (F2F3F4F5) by the same conservative mutational strategy described above and analyzed the effects of simultaneously removing multiple N-glycans on the fusogenicity of NiV-F in 293T cells. In order to account for variability in CSE for the N-glycan mutants, we compared CSE and cell-cell fusion for WT NiV-F against those of the above-mentioned NiV-F N-glycan mutants (Fig. 3A). The CSE of these N-glycan mutants was measured by flow cytometry as described for Fig. 1D and normalized to the mean fluorescence intensity obtained for WT NiV-F, which was set at 100%. Similarly, fusogenicity for the N-glycan mutants was quantified and normalized to the number of nuclei in syncytia formed by WT NiV-F, which was again set at 100%. We wish to emphasize that the amount of DNA used and the cell surface expression observed were in the linear portion of the dose-response curve shown in Fig. 2C and D. Thus, a fusion-to-CSE ratio is a reasonable indicator of fusogenicity that might account for the differential surface expression among the N-glycan mutants

TABLE 1. Fusion/CSE ratios for WT NiV-F and the N-glycan mutant proteins[a]

NiV-F Env	Fusion/CSE ratio
F	1
F2	1
F3	6.5
F4	1.9
F5	3.4
F2F3	4.8
F2F4	6.8
F2F5	4.4
F3F4	17.7
F3F5	6.6
F4F5	8.6
F2F3F5	3.9
F2F4F5	47.3
F2F3F4F5	4.6

[a] The fusogenicity and cell surface expression of the N-glycan mutants were within the linear range of our assay described for Fig. 2B to E. Therefore, a reasonable indicator of fusogenicity that takes into account the differential expression levels among the various N-glycan mutants is the fusion-to-CSE ratio. Both fusion (nuclei in syncytia per field) and CSE (mean channel fluorescent intensity) levels of the N-glycan mutants were normalized to that of WT NiV-F, which was set at 100%. The ratios of the normalized fusion and CSE values for each mutant were then calculated. By definition, the fusion and CSE ratio for WT NiV-F would be 1.0 (100%/100%).

(Table 1). In general, removal of multiple N-glycans had a greater effect on fusion than did removal of individual N-glycans. For example, while only the F3 and F5 individual N-glycan mutants showed significantly increased fusion (>2-fold) compared to WT NiV-F, all of the multiple N-glycan mutants had fusion/CSE ratios more than twice that of WT NiV-F (Table 1) (compare Fig. 2B with 3A).

In addition, removal of some N-glycans clearly had synergistic effects on fusion efficiencies. For example, while the F2 and F4 single N-glycan mutants had fusogenicities close to that of WT NiV-F (fusion/CSE ratio, <2), the F2 and F4 double mutant had a significantly higher fusion/CSE ratio than did WT NiV-F (Table 1, fusion/CSE ratio of 6.8). Remarkably, the F2F4F5 triple mutant had one of the highest levels of cell-cell fusion despite having one of the lowest levels of CSE (Fig. 3A). Since this F2F4F5 mutant had much lower CSE levels than the WT NiV-F protein did, these data suggest that removal of N-glycosylation can result in a more easily triggered NiV-F protein, such that fusion can occur at much lower levels of surface expression. Interestingly, CSEs of all multiple N-glycan mutants that did not contain the F4 mutation were similar to that of WT NiV-F protein (Fig. 3A, last four mutants on the right), while all the mutants that included the F4 mutation were expressed at lower levels than WT NiV-F protein was (Fig. 3A, first five mutants on the left). The immediate amino acid environment surrounding the F4 N-glycan site has been shown to be important for proper transport and cell surface expression (21). However, our data also show that the F4 N-glycan, in a variable combination with other N-glycans, plays an important role in efficient expression of NiV-F and/or transport of the protein to the cell surface.

Removal of N-glycans also enhances viral entry. We then asked if the hyperfusogenicity observed for the NiV-F N-glycan mutants translated into an increase in viral entry. As NiV is a biosafety level 4 pathogen, we have established a viral entry assay using NiV-F/G pseudotyped onto a VSV reporter lacking its own envelope glycoprotein (VSV-ΔG) (25) and expressing the *Renilla* luciferase gene. To perform an unbiased comparison, we pseudotyped only single or multiple NiV-F N-glycan mutants that showed WT CSE levels (Fig. 2B and 3A) and measured their infectivities on Vero cells over a broad range of viral dilutions. In addition, we quantified the amount of our input virus by measuring the number of input VSV genome copies via quantitative reverse transcription-PCR and also monitored the amount of envelope incorporation into our pseudotyped virions (Fig. 3D). For clarity, the infectivities of WT NiV-F compared to those of the single and multiple N-glycan mutants are shown separately in Fig. 3B and 3C, respectively. At high viral inocula (10^6 to 10^7 viral genomes/ml), little or no difference in infectivity was observed between reporter viruses bearing WT NiV-F and those bearing the various N-glycan mutants. However, at lower viral inocula (10^4 to 10^5 viral genomes/ml), when the amount of virus used was not saturating, most of the N-glycan mutants recapitulated the hyperfusogenic phenotype seen in the syncytium formation assays. Note that the *y* axis in Fig. 3B and C indicating viral entry efficiency as shown by luciferase reporter activity shows a log scale. Thus, the F3 and F5 (Fig. 3B, second and fourth graphs) and the F2F3 and F2F5 (Fig. 3C, first and second graphs) NiV-F mutants had viral entry efficiencies up to four- to sixfold higher than that of WT NiV-F (at 10^4 input viral genomes/ml), similar to what was observed in the cell-cell fusion assay (Fig. 2B and 3A). The increase in viral entry efficiency was not as marked for two mutants (F3F5 and F2F3F5), likely due to the low level of NiV-F incorporation into the pseudotyped virion (Fig. 3D, last lanes). We also noted that some mutants, such as F2F3, had levels of entry up to sixfold higher than that of WT NiV-F, despite having comparatively lower levels of NiV-F incorporation (Fig. 3D). Thus, although NiV-F incorporation was uneven among some of our N-glycan mutants, the fact that the N-glycan mutants exhibited at least wild-type or greater levels of viral entry despite, in some cases, significantly lowered levels of envelope incorporation suggests that the hyperfusogenic phenotype of the NiV-F N-glycan mutants is translated into increases in viral entry. It is important that the data in Fig. 1B and Fig. 3D show that F expressed at the cell surface or incorporated into virions (which is by definition "cell surface" F) is cleaved as efficiently as or less efficiently than, but never more efficiently than, wild-type F. Thus, the fusion/CSE ratios in Table 1 and the viral entry results in Fig. 3B and Fig. 3C are likely the minimal estimates of their relative fusogenicities.

Surprisingly, the F2 mutant, which did not have a hyperfusogenic phenotype in the cell-cell fusion assay (Fig. 2A and B), showed up to a fourfold increase in viral entry efficiency (Fig. 3B) that was apparent at low viral inocula, suggesting differences in sensitivities between the two assays. Overall, these data show that specific N-glycans on NiV-F play a critical role in limiting cell-cell fusion as well as viral entry efficiencies.

N-glycans are important for protecting NiV-F from NAbs. If removal of N-glycans on NiV-F generally resulted in greater fusion and entry efficiencies (Fig. 2), what is (are) the biological role(s) of N-glycosylation on NiV-F? Do N-glycans in the NiV-F protein have the function of suppressing cell-cell fusion so that the host can survive until the virus can replicate suffi-

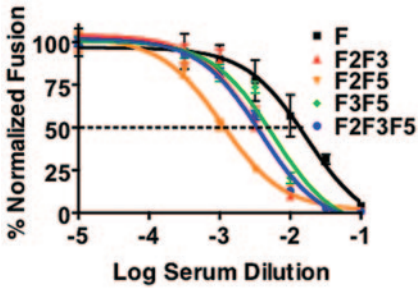

FIG. 4. N-glycans protect NiV from neutralizing antibodies. Cell-cell fusion mediated by WT NiV-F and the indicated mutants was differentially inhibited by a polyclonal anti-NiV-F-specific antiserum. The fusion assay was performed in 293T cells as described above, except that serial dilutions of the anti-NiV-F antiserum were incubated with the transfected cells during the overnight incubation. The amount of fusion seen in the absence of anti-NiV-F antiserum was normalized to 100%. The inhibition curves were regressed, and the IC_{50}s were calculated using GraphPad PRISM. Data are shown as normalized averages ± standard deviations from two separate experiments.

ciently, and/or is there any other biological function for NiV-F N-glycans? The concept of a "glycan shield" has been posited to explain the ability of certain viruses to constantly thwart neutralizing antibody (NAb) responses (8, 27, 42). Thus, we asked if N-glycans on NiV-F might play a similar role in protecting NiV from NAb responses.

We examined if N-glycan mutants were more sensitive to antibody-mediated neutralization than WT NiV-F was in the context of a syncytium formation assay. The indicated mutants (Fig. 4) were specifically chosen as they had increased fusogenic capacities but CSE levels similar to those of WT NiV-F (Fig. 3A, last four mutants on the right). Thus, any differences in neutralization sensitivity observed in the cell-cell fusion assay would likely not result from differences in CSE. Anti-NiV-F antisera more readily neutralized fusion promoted by the NiV-F N-glycan mutants than fusion promoted by WT NiV-F. A 3- to 20-fold increase in neutralization sensitivity was observed as the 50% inhibitory serum dilution for WT NiV-F was 0.02, while those for F3F5, F2F3, F2F3F5, and F2F5 were 0.06, 0.03, 0.03, and 0.001, respectively (Fig. 4). In general, the relative differences in inhibition sensitivities observed in the cell-cell fusion assays correlated with the neutralization sensitivities observed in viral entry assays (data not shown), for example, with the F2F5 mutant also being the most sensitive to antibody neutralization. However, since envelope incorporation was uneven in these pseudotyped virions (Fig. 3D), and envelope spike density can affect neutralization sensitivity, we refrained from definitive conclusions regarding the neutralization sensitivities in these viral entry assays.

Hyperfusogenic NiV-F N-glycan mutants are more resistant to fusion inhibition by a reagent that prevents six-helix bundle formation and exhibit faster fusion kinetics than WT NiV-F. We then proceeded to examine the potential mechanisms that contribute to the hyperfusogenic phenotypes exhibited by the NiV-F N-glycan mutants. Peptides representing the C-terminal heptad repeat region (HR2) of NiV-F (5), other paramyxoviruses (47), or HIV-1 (43) have been shown to inhibit syncytium formation, presumably by interfering with six-helix bundle formation, a canonical pathway for fusion that is used by all class I fusion proteins (10). The rate of six-helix bundle formation has been linked to fusogenicity in other viruses (1, 11, 12). Thus, we tested the sensitivity of WT NiV-F or NiV-F N-glycan mutants to fusion inhibition by a reagent that mimicked the NiV-HR2 peptide (NiV-HR2-Fc). The NiV-F or HIV-gp41 fusion protein HR2 region was linked to the Fc constant region of human IgG1 and placed downstream of a kappa/lambda signal sequence for efficient secretion into the supernatant to make the NiV-HR2-Fc or HIV-HR2-Fc protein, respectively. A protein similar to HIV-HR2-Fc was previously shown to be functionally equivalent to the cognate HIV-1 HR2 peptide (36). We found that NiV-HR2-Fc specifically inhibited NiV fusion and not HIV entry, while the converse was true for HIV-HR2-Fc (Fig. 5A). Thus, using NiV-F-HR2-Fc in fusion inhibition experiments, we observed that the NiV-F N-glycan mutants exhibited a three- to sevenfold-greater resistance to NiV-HR2-Fc than did WT NiV-F (Fig. 5B). For example, while the 50% inhibitory concentration (IC_{50}) of NiV-HR2-Fc for WT NiV-F was 3.3 nM, the IC_{50} values for the N-glycan mutants ranged from 8 nM to >20 nM (Fig. 5B).

To determine if the greater resistance to NiV-HR2-Fc is due to a faster transition to six-helix bundle formation or to accessibility differences due to conformational alterations, we measured the fusion kinetics mediated by WT NiV-G and NiV-F or the indicated N-glycan mutants. A faster transition to six-helix bundle formation during fusion pore formation would likely lead to an increased rate of fusion, which can be measured using a β-lactamase reporter cell-cell fusion assay that can measure fusion kinetics in real time (18, 31). We found that cells expressing three of the four NiV-F N-glycan mutants analyzed showed faster fusion kinetics and fused to a greater extent than did cells expressing WT NiV-F (Fig. 5C). F2F3, F3F5, and F2F3F5 mutants showed the highest rates of fusion, while the F2F5 mutant fused more slowly, but to the same extent as cells expressing WT NiV-F (Fig. 5C). However, we cannot rule out the possibility that the F2F5 N-glycan mutant will eventually reach a higher level of fusion in a longer time course. In general, our results support the model that the hyperfusogenic N-glycan mutants undergo a faster transition to the six-helix bundle during fusion pore formation, resulting in increased fusion kinetics.

The data thus far suggest that specific glycans on unique sites in NiV-F preferentially affect fusogenicity versus protection from neutralization antibodies. Thus, in agreement with single N-glycan removal in mutant F3 in Fig. 2B, all multiple N-glycan mutants missing the F3 N-glycan (F2F3, F3F5, and F2F3F5) had the highest rate of fusion (Fig. 5C), the highest resistance to NiV-HR2-Fc (Fig. 5B), and the highest level of syncytium formation (Fig. 3A), while the F2F5 N-glycan mutant had the lowest rate of fusion, was the most sensitive to NiV-HR2-Fc, and also was the most sensitive to antibody neutralization. Thus, of the N-glycans examined, the F3 N-glycan appears to preferentially affect fusion, while the F2 and F5 N-glycans appear to be more important for protection against NAb.

Fusogenicity of NiV-F is inversely correlated with the relative avidity of F/G interactions. Interactions between the fusion and attachment proteins of many paramyxoviruses play critical roles in promoting membrane fusion, and we had previously shown by a reciprocal coimmunoprecipitation assay

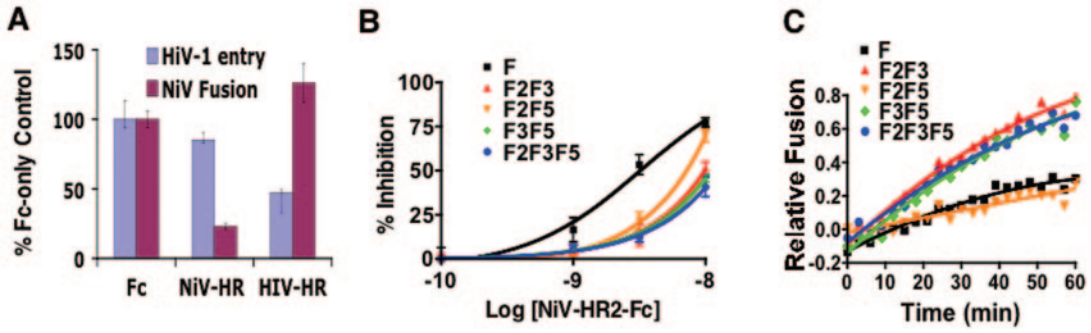

FIG. 5. Hyperfusogenicity of the N-glycan mutants is correlated with the sensitivity to heptad repeat region inhibition and the rate of six-helix bundle formation. (A) A novel NiV-heptad-repeat-human-Fc immunoadhesin (NiV-HR2-Fc) inhibited NiV envelope-induced fusion (in 293T cells) but not entry of HIV-1 virions (in TZM-bl HeLa-based luciferase reporter cells) (9). A similar HIV-HR2-Fc protein inhibited HIV-1 virus entry but not NiV envelope-induced fusion. Data are presented as percentages of Fc-only control (averages ± standard errors from three separate experiments. (B) The sensitivity of NiV envelope-mediated fusion to inhibition by NiV-HR2-Fc is shown for WT NiV-F and the indicated N-glycan mutants. For each fusion protein, the amount of fusion in the absence of any inhibitor is set at 0% inhibition. One representative experiment out of two is shown. Error bars indicate standard deviations. (C) Fusion kinetics of WT or mutant NiV-F proteins. NiV-G was expressed with the indicated NiV fusion proteins in effector PK13 cells, and the relative rate of fusion was assessed on target 293T cells loaded with CCF2 dye (see Materials and Methods). Relative fusion is the ratio of blue to green fluorescence obtained with NiV-G- and NiV-F-transfected effectors minus the ratio of background blue and green fluorescence obtained with empty-vector (pcDNA3)-transfected cells. Each data point is an average from three independent experiments. Linear regression on data points was performed with GraphPad PRISM.

that NiV-F and NiV-G interact (17). Models for paramyxoviruses have been proposed where receptor binding triggers conformational changes in the attachment protein, leading to disruption of its association with the fusion protein, which can then be activated to undergo fusion peptide exposure (38, 49). Moreover, for NDV, it has been shown that the HN attachment protein alters the conformation of the F protein at the cell surface (20). Also, for measles virus, weakening of the F/H cytoplasmic tail interaction by addition of an epitope tag to the cytoplasmic tail of the H attachment glycoprotein resulted in increased fusogenicity (28). These models predict that hyperfusogenic phenotypes may result from weaker interactions between NiV-F mutants and NiV-G, allowing greater NiV-F/NiV-G dissociation after receptor binding. Therefore, we asked whether the relative avidity of NiV-F/NiV-G interactions correlated with the fusogenicity of the N-glycan mutants.

We coexpressed NiV-G with WT NiV-F or the aforementioned N-glycan mutants in permissive 293T cells and determined the relative avidities of NiV-F and NiV-G interactions by reciprocal coimmunoprecipitation (Fig. 6A and B). That is, lysates immunoprecipitated with anti-NiV-G were Western blotted for NiV-F, while lysates immunoprecipitated with NiV-F were Western blotted for NiV-G (Fig. 6A). We reasoned that the avidity of F and G interaction would be reflected in the efficiency of the coimmunoprecipitation. Co-IP NiV-G or NiV-F proteins were also normalized against their total amounts in the cell lysates to account for the various expression levels of WT or mutant NiV-F in any single experiment. Thus, we calculated a ratio between the levels of co-IP NiV-F and the corresponding amount of NiV-F in total cell lysate (Fig. 6A, left panel). For example, if the amount of co-IP NiV-F was 150 densitometric units and the amount of NiV-F directly immunoprecipitated from the cell lysate was 200 densitometric units, the F/G co-IP ratio would be 0.75. This ratiometric value was arbitrarily set to 1.0 to indicate the relative avidity of the WT NiV-F and NiV-G interaction (Fig. 6B). Using this scale, a value of less than 1.0 would indicate a decreased avidity in F/G interaction relative to the WT proteins. Similar normalizations were done for NiV-G co-IP with the different NiV-F WT or mutant proteins (Fig. 6A, right panel, and also annotated in Fig. 6B). Thus, the relative avidities between NiV-F and NiV-G can be represented by two independent sets of ratios from Fig. 6A (a/b and c/d; normalized ratiometric values are shown in Fig. 6B).

Next, we plotted the relative avidities of NiV-G's interactions with WT NiV-F, or the indicated N-glycan mutants, against their fusogenicities (fusion index), as determined for the data shown in Fig. 3A and Table 1. Regardless of how we quantified the relative avidity between NiV-F and NiV-G (amount of NiV-F co-IP with NiVG [a/b] or the amount of NiV-G co-IP with NiV-F [c/d]), we obtained significant negative correlations ($r^2 = 0.88$, $P = 0.008$, and $r^2 = 0.98$, $P = 0.0006$) between the avidity of F and G interaction and the fusogenicity of the NiV-F protein (Fig. 6C). Thus, for example, the NiV-F mutant (F3F5) with the lowest relative avidity of F and G interaction (0.12 to 0.14) was also the most fusogenic NiV-F mutant examined (fusion/CSE ratio, >7). These results suggest that the effects of N-glycans on limiting fusogenicity are linked to the increasing avidity of the F/G interactions and provide direct support for the model (38, 49) where dissociation of the attachment protein from the fusion protein is required for fusion peptide exposure and subsequent membrane fusion.

DISCUSSION

N-glycans on other paramyxovirus fusion proteins are known to be required for proper expression, conformational integrity, and efficient fusogenicity of the protein (13, 19, 35, 40). Surprisingly, we show in this report that many of the N-glycans on NiV-F are not required for conformational integrity and actually reduce fusion efficiency but protect the fusion protein from neutralizing antibodies. Indeed, removal of multiple N-glycans on NiV-F resulted in hyperfusogenic phenotypes, and the pres-

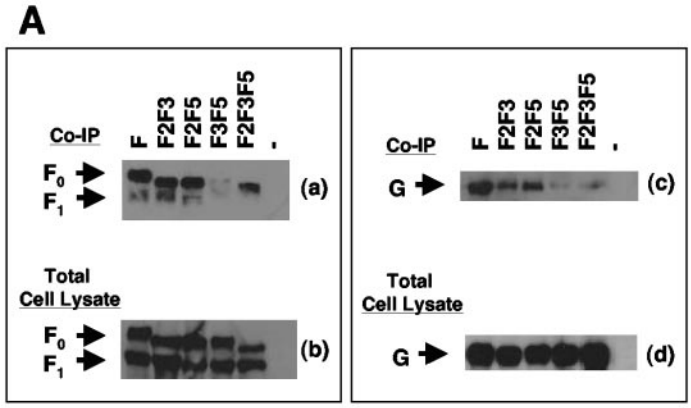

B

Env Protein	Avidity of F/G Interactions (a/b)	Avidity of F/G Interactions (c/d)
F	1.0	1.0
F2F3	0.33	0.43
F2F5	0.74	0.49
F3F5	0.12	0.14
F2F3F5	0.29	0.30

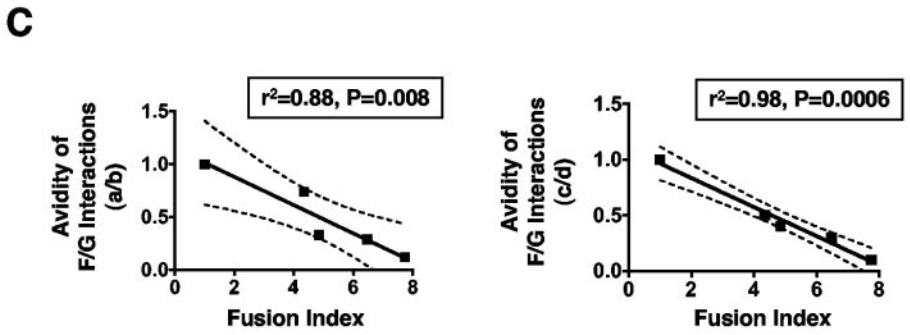

FIG. 6. Fusogenicity is inversely correlated with the avidity of F/G interactions. (A) Reciprocal coimmunoprecipitation of NiV-F and NiV-G. Cell lysates of 293T cells transfected with WT NiV-G and NiV-F or the indicated N-glycan mutants were immunoprecipitated using rabbit anti-NiV-G-specific antisera or rabbit anti-F-specific antisera. The immunoprecipitates containing directly immunoprecipitated and coimmunoprecipitated proteins were split in half and analyzed by Western blotting. Left panels (a and b) were blotted with mouse anti-AU1 to detect NiV-F, and right panels (c and d) were blotted with mouse antihemagglutinin to detect NiV-G. (B) Relative avidities of NiV-G interactions for the WT or mutant NiV-F proteins. The amounts of co-IP NiV-F and NiV-G in panel A (a and c, respectively) were quantified by densitometry as described in the text using a VersaDoc Imaging System (Bio-Rad). The avidity of F/G interactions is represented by the ratio of the amount of NiV-F protein coimmunoprecipitated with anti-NiV-G antisera (a) to the amount of NiV-F directly immunoprecipitated from total cell lysates (b) in panel A or the ratio of the amount of NiV-G protein coimmunoprecipitated with anti-NiV-F antisera (c) to the amount of NiV-G protein directly immunoprecipitated from total cell lysates (d). (C) The ratiometric values representing F/G interaction avidities from panel B were plotted against the fusion/CSE ratios (fusion index) from Table 1. Pearson correlation analysis was performed using GraphPad PRISM.

ence of N-glycans on NiV-F likely reduced the rate of six-helix bundle formation, resulting in slower fusion kinetics. The hyperfusogenic phenotypes of the NiV-F N-glycan mutants were most marked in 293T cells, slightly less apparent in Vero cells, and least apparent in MDCK cells. This is consistent with the slight increase in fusogenicity noted for the F3 and F5 N-glycan mutants in MDCK cells by Moll et al. (21). Cell-type-specific glycosylation (the type and quantity of glycans that are added on) and expression levels likely account for these differences. Indeed, Western blotting of NiV-F produced in 293T cells versus that produced in MDCK cells indicate that they migrate with slightly different mobilities, suggestive of glycosylation differences (data not shown).

N-glycans on viral envelope glycoproteins can "shield" viruses from NAbs. To our knowledge, the role of N-glycans in viral escape from NAb has not been documented for paramyxoviruses but is well documented for viruses such as HIV (42), SIV (32), EIAV (33), HepB (16), and influenza virus (37) (reviewed in reference 27). Here, we uncovered a role for N-glycans on the NiV fusion protein as a "glycan shield" against NAb (Fig. 4). The "unshielded" NiV-F N-glycan mutants were more neutralizable by polyclonal anti-NiV-F than was fully glycosylated NiV-F. Future testing of these N-glycan mutans against convalescent-phase sera from NiV-infected patients will help determine the veracity of this "glycan shield" hypothesis. Our results may have implications for NiV vaccine development, as this increased neutralization sensitivity may be a result of increased peptide epitope exposure. Selective deglycosylation and the resultant increased epitope exposure may result in more potent and/or broader neutralizing antibody responses, as has been observed for SIV (32), EIAV (33), and HepB (16). Thus, we speculate that these neutralization-sensitive N-glycan mutants may elicit improved NAb responses.

We found that N-glycans on the NiV fusion protein (NiV-F) "protected" NiV-F against neutralization by NAb (Fig. 4). However, removal of these N-glycans, in general, also greatly increased its fusogenicity (Fig. 2 and 3). These varied roles for N-glycans on NiV-F contrast sharply with the role of N-glycans on other paramyxoviral glycoproteins, as removal of specific N-glycans from the Newcastle disease, measles, and Sendai virus F proteins results in severe defects in fusion (13, 19, 35).

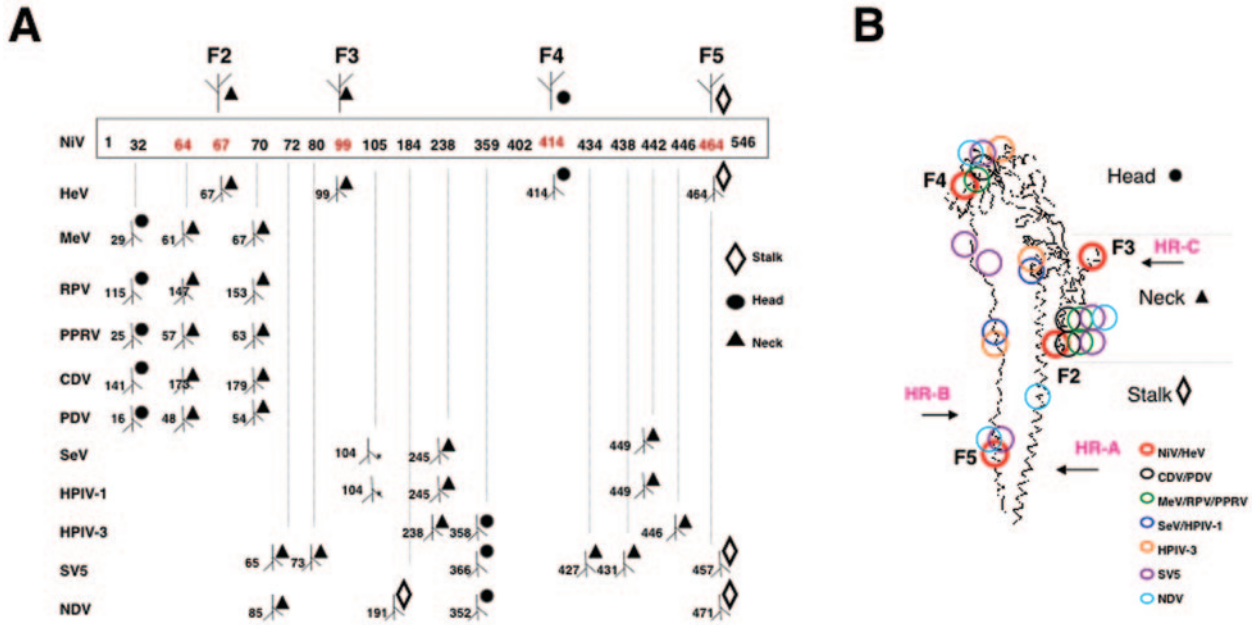

FIG. 7. Comparison of the primary and tertiary structures of the NiV, HeV, MeV, RPV, PPRV, CDV, PDV, SeV, HPIV-1, HPIV-3, SV5, and NDV paramyxovirus F proteins. The 3-D structure of each paramyxovirus F protein was modeled based on the solved crystal structure of the HPIV-3 F protein (see Materials and Methods), and the N-linked glycosylation sites were mapped onto the predicted structure. (A) Linear comparison of the 12 sequences based on Clustal W multiple sequence alignments. The amino acid positions (not to scale) of the potential N-linked glycosylation sites in NiV-F are shown in red in the top sequence representation. Actual glycan attachment sites are indicated by a branched tree symbol at the amino acid position. Positions of the other paramyxovirus F proteins are shown below the NiV-F sequence, with the amino acid sequence position indicated to the left of the glycan symbol and its position in the predicted 3-D structure on the right; circles, triangles, and diamonds represent glycans located in the head, neck, and stalk region, respectively, of the predicted or actual (for HPIV3) 3-D structure. Asterisks denote N-linked glycosylation sites that could not be structurally mapped. (B) Carbon backbone representation of the HPIV-3 F structure (48), representing the general overall fold of the paramyxovirus F protein. N-linked glycosylation sites which can be mapped onto this structure using the threading methodology described in Materials and Methods are indicated by circles; see the key in the figure. The heptad repeat regions (HR-A, HR-B, and HR-C) and head, neck, and stalk regions are also indicated.

Nevertheless, our findings that the hyperfusogenic NiV-F N-glycan mutants also displayed increased fusion kinetics and increased resistance to a novel NiV-F heptad repeat fusion inhibitory protein (NiV-HR2-Fc) (Fig. 5) are consistent with the mechanisms underlying the hyperfusogenic phenotypes in other viruses with class I fusion proteins. For example, the hyperfusogenic V3 loop and cytoplasmic tail of HIV-1 envelope glycoprotein mutants also show faster fusion kinetics and display increased resistance to heptad repeat peptide inhibition (1, 30). We note that while hyperfusogenic phenotypes in viruses with class I fusion proteins are commonly identified, it is less common, if not novel, to find a whole class of mutations, such as removal of N-glycans, that result additively or synergistically in hyperfusogenicity. We cannot formally exclude the possibility that the resistance of our N-glycan mutants to heptad repeat inhibition is due to conformational differences that result in the heptad repeat region binding sites being less accessible. Therefore, it remains to be determined how N-glycans on NiV-F actually modulate the kinetics of fusion. Do the N-glycans stabilize the metastable prefusogenic conformation of NiV-F, or do they physically impede six-helix bundle formation due to their bulky hydrophilic nature?

To obtain further insights into the relatively novel roles for N-glycans in NiV-F, we compared the primary and tertiary structures of 12 paramyxovirus fusion proteins. The three-dimensional (3-D) structure of each paramyxovirus F protein was modeled based on the solved crystal structure of the HPIV-3 F protein (see Materials and Methods), and the established N-linked glycosylation sites were mapped onto the predicted structure (Fig. 7). Our modeling of the NiV-F N-glycan sites showed that while the F2, F3, and F4 N-glycan sites do not align with the primary sequence of other paramyxoviruses (except for HeV) (Fig. 7A), the F2 and F4 N-glycan sites clustered in the similar globular head and neck regions with N-glycans from many other paramyxoviruses (Fig. 7B) (40). The F5 N-glycan site aligned only with SV5 and NDV (in addition to HeV) in primary sequence and also mapped to the HR-B region, a relatively uncommon site for N-glycans. Despite this similarity, the N-glycans in the HR-B region of the SV5 and NDV F proteins seem to be important for efficient cleavage and cell surface expression (3) or fusogenicity (19). This is clearly different from the NiV/HeV F5 N-glycan mutation, which enhances fusogenicity, as seen from our data for NiV and those of Carter et al. for HeV (7). The modulating parameter(s) of the relatively unique nature of the F5 N-glycan remains to be determined.

However, we note that the NiV/HeV F3 N-glycan mapped to a unique position in the HR-C region. It is interesting that the F3 NiV-F protein had the highest level of fusogenicity of all the single N-glycan mutant proteins. To our knowledge, the HR-C region has not been previously implicated in the fusion process, but our data suggest that a bulky hydrophilic structure in

this area clearly inhibits fusion, perhaps by impeding the conformational changes that NiV-F undergoes between the pre- and postfusion states.

Although some level of association is generally required between the fusion and attachment proteins of paramyxoviruses in order for productive fusion to occur (15, 23), current models suggest that dissociation of the attachment protein from the fusion protein after receptor engagement is required for efficient fusion peptide exposure (38, 49). These models predict that a greater propensity for attachment protein/fusion protein dissociation might lead to greater fusion peptide exposure and thus increased fusogenicity. Indeed, our results provide direct experimental evidence for this model. The fusogenicity of the N-glycan mutants was negatively correlated with the relative avidity of F/G interactions as quantified by coimmunoprecipitation (Fig. 6). Higher levels of shedding of the attachment subunit from the fusion glycoprotein subunit have been linked to higher fusogenicity in viruses such as HIV and Moloney murine leukemia virus, where similar models of attachment protein dissociation from the fusion protein prior to fusion peptide exposure have been suggested (2, 11, 22).

It remains to be determined how N-glycans on NiV-F actually stabilize F/G interactions and why N-glycans on NiV-F appear to play a different role than N-glycans on the fusion proteins of other paramyxoviruses. Do the unique roles of the NiV-F N-glycans in NiV entry contribute to the unusual pathogenicity of the virus? Moreover, is there an advantage of down regulating the fusogenic capacity of the NiV-F protein by N-glycan addition so that the virus does not kill the host before it can successfully spread? Can the infectivity of NiV differ in vivo when produced in cell types with differential glycosylation machinery? Answers to these questions will enhance our understanding of the pathobiology of this deadly emerging virus.

ACKNOWLEDGMENTS

This work was supported by NIH grants AI059051 to B.L., AI060694 to L.G.B. and B.L., and AI61824 to E.L.L. B.L. is a Charles E. Culpepper Medical Scholar supported by the Rockefeller Brothers Fund and a recipient of the Burroughs Wellcome Fund Career Development Award. J.A.F., M.C.W., and O.A.N. are supported by NIH grants GM08042 and AI07323 and an NIH NRSA grant, respectively. We acknowledge support from the UCLA AIDS Institute and the CFAR flow cytometry core supported by NIH grants CA16042 and AI28697.

REFERENCES

1. **Abrahamyan, L. G., S. R. Mkrtchyan, J. Binley, M. Lu, G. B. Melikyan, and F. S. Cohen.** 2005. The cytoplasmic tail slows the folding of human immunodeficiency virus type 1 Env from a late prebundle configuration into the six-helix bundle. J. Virol. **79:**106–115.
2. **Aguilar, H. C., W. F. Anderson, and P. M. Cannon.** 2003. Cytoplasmic tail of Moloney murine leukemia virus envelope protein influences the conformation of the extracellular domain: implications for mechanism of action of the R peptide. J. Virol. **77:**1281–1291.
3. **Bagai, S., and R. A. Lamb.** 1995. Individual roles of N-linked oligosaccharide chains in intracellular transport of the paramyxovirus SV5 fusion protein. Virology **209:**250–256.
4. **Bonaparte, M. I., A. S. Dimitrov, K. N. Bossart, G. Crameri, B. A. Mungall, K. A. Bishop, V. Choudhry, D. S. Dimitrov, L. F. Wang, B. T. Eaton, and C. C. Broder.** 2005. Ephrin-B2 ligand is a functional receptor for Hendra virus and Nipah virus. Proc. Natl. Acad. Sci. USA **102:**10652–10657.
5. **Bossart, K. N., B. A. Mungall, G. Crameri, L. F. Wang, B. T. Eaton, and C. C. Broder.** 2005. Inhibition of Henipavirus fusion and infection by heptad-derived peptides of the Nipah virus fusion glycoprotein. Virol. J. **2:**57. [Online.]
6. **Bossart, K. N., L. F. Wang, B. T. Eaton, and C. C. Broder.** 2001. Functional expression and membrane fusion tropism of the envelope glycoproteins of Hendra virus. Virology **290:**121–135.
7. **Carter, J. R., C. T. Pager, S. D. Fowler, and R. E. Dutch.** 2005. Role of N-linked glycosylation of the Hendra virus fusion protein. J. Virol. **79:**7922–7925.
8. **Cheng-Mayer, C., A. Brown, J. Harouse, P. A. Luciw, and A. J. Mayer.** 1999. Selection for neutralization resistance of the simian/human immunodeficiency virus SHIVSF33A variant in vivo by virtue of sequence changes in the extracellular envelope glycoprotein that modify N-linked glycosylation. J. Virol. **73:**5294–5300.
9. **Derdeyn, C. A., J. M. Decker, J. N. Sfakianos, X. Wu, W. A. O'Brien, L. Ratner, J. C. Kappes, G. M. Shaw, and E. Hunter.** 2000. Sensitivity of human immunodeficiency virus type 1 to the fusion inhibitor T-20 is modulated by coreceptor specificity defined by the V3 loop of gp120. J. Virol. **74:**8358–8367.
10. **Eckert, D. M., and P. S. Kim.** 2001. Mechanisms of viral membrane fusion and its inhibition. Annu. Rev. Biochem. **70:**777–810.
11. **Gallo, S. A., C. M. Finnegan, M. Viard, Y. Raviv, A. Dimitrov, S. S. Rawat, A. Puri, S. Durell, and R. Blumenthal.** 2003. The HIV Env-mediated fusion reaction. Biochim. Biophys. Acta **1614:**36–50.
12. **Gallo, S. A., A. Puri, and R. Blumenthal.** 2001. HIV-1 gp41 six-helix bundle formation occurs rapidly after the engagement of gp120 by CXCR4 in the HIV-1 Env-mediated fusion process. Biochemistry **40:**12231–12236.
13. **Hu, A., T. Cathomen, R. Cattaneo, and E. Norrby.** 1995. Influence of N-linked oligosaccharide chains on the processing, cell surface expression and function of the measles virus fusion protein. J. Gen. Virol. **76:**705–710.
14. **Lam, S. K.** 2003. Nipah virus—a potential agent of bioterrorism? Antivir. Res. **57:**113–119.
15. **Lamb, R. A.** 1993. Paramyxovirus fusion: a hypothesis for changes. Virology **197:**1–11.
16. **Lee, J., J. S. Park, J. Y. Moon, K. Y. Kim, and H. M. Moon.** 2003. The influence of glycosylation on secretion, stability, and immunogenicity of recombinant HBV pre-S antigen synthesized in Saccharomyces cerevisiae. Biochem. Biophys. Res. Commun. **303:**427–432.
17. **Levroney, E. L., H. C. Aguilar, J. A. Fulcher, L. Kohatsu, K. E. Pace, M. Pang, K. B. Gurney, L. G. Baum, and B. Lee.** 2005. Novel innate immune functions for galectin-1: galectin-1 inhibits cell fusion by Nipah virus envelope glycoproteins and augments dendritic cell secretion of proinflammatory cytokines. J. Immunol. **175:**413–420.
18. **Lineberger, J. E., R. Danzeisen, D. J. Hazuda, A. J. Simon, and M. D. Miller.** 2002. Altering expression levels of human immunodeficiency virus type 1 gp120-gp41 affects efficiency but not kinetics of cell-cell fusion. J. Virol. **76:**3522–3533.
19. **McGinnes, L., T. Sergel, J. Reitter, and T. Morrison.** 2001. Carbohydrate modifications of the NDV fusion protein heptad repeat domains influence maturation and fusion activity. Virology **283:**332–342.
20. **McGinnes, L. W., K. Gravel, and T. G. Morrison.** 2002. Newcastle disease virus HN protein alters the conformation of the F protein at cell surfaces. J. Virol. **76:**12622–12633.
21. **Moll, M., A. Kaufmann, and A. Maisner.** 2004. Influence of N-glycans on processing and biological activity of the Nipah virus fusion protein. J. Virol. **78:**7274–7278.
22. **Moore, J. P., J. A. McKeating, R. A. Weiss, and Q. J. Sattentau.** 1990. Dissociation of gp120 from HIV-1 virions induced by soluble CD4. Science **250:**1139–1142.
23. **Morrison, T. G.** 2003. Structure and function of a paramyxovirus fusion protein. Biochim. Biophys. Acta **1614:**73–84.
24. **Navarro-Sanchez, E., R. Altmeyer, A. Amara, O. Schwartz, F. Fieschi, J. L. Virelizier, F. Arenzana-Seisdedos, and P. Despres.** 2003. Dendritic-cell-specific ICAM3-grabbing non-integrin is essential for the productive infection of human dendritic cells by mosquito-cell-derived dengue viruses. EMBO Rep. **4:**723–728.
25. **Negrete, O. A., E. L. Levroney, H. C. Aguilar, A. Bertolotti-Ciarlet, R. Nazarian, S. Tajyar, and B. Lee.** 2005. EphrinB2 is the entry receptor for Nipah virus, an emergent deadly paramyxovirus. Nature **436:**401–405.
26. **Olofsson, S., and J. E. Hansen.** 1998. Host cell glycosylation of viral glycoproteins—a battlefield for host defence and viral resistance. Scand. J. Infect. Dis. **30:**435–440.
27. **Pikora, C. A.** 2004. Glycosylation of the ENV spike of primate immunodeficiency viruses and antibody neutralization. Curr. HIV Res. **2:**243–254.
28. **Plemper, R. K., A. L. Hammond, D. Gerlier, A. K. Fielding, and R. Cattaneo.** 2002. Strength of envelope protein interaction modulates cytopathicity of measles virus. J. Virol. **76:**5051–5061.
29. **Rasmussen, T. B., A. Uttenthal, J. Fernandez, and T. Storgaard.** 2005. Quantitative multiplex assay for simultaneous detection and identification of Indiana and New Jersey serotypes of vesicular stomatitis virus. J. Clin. Microbiol. **43:**356–362.
30. **Reeves, J. D., S. A. Gallo, N. Ahmad, J. L. Miamidian, P. E. Harvey, M. Sharron, S. Pohlmann, J. N. Sfakianos, C. A. Derdeyn, R. Blumenthal, E. Hunter, and R. W. Doms.** 2002. Sensitivity of HIV-1 to entry inhibitors correlates with envelope/coreceptor affinity, receptor density, and fusion kinetics. Proc. Natl. Acad. Sci. USA **99:**16249–16254.
31. **Reeves, J. D., J. L. Miamidian, M. J. Biscone, F. H. Lee, N. Ahmad, T. C. Pierson, and R. W. Doms.** 2004. Impact of mutations in the coreceptor

binding site on human immunodeficiency virus type 1 fusion, infection, and entry inhibitor sensitivity. J. Virol. **78:**5476–5485.
32. **Reitter, J. N., R. E. Means, and R. C. Desrosiers.** 1998. A role for carbohydrates in immune evasion in AIDS. Nat. Med. **4:**679–684.
33. **Salinovich, O., S. L. Payne, R. C. Montelaro, K. A. Hussain, C. J. Issel, and K. L. Schnorr.** 1986. Rapid emergence of novel antigenic and genetic variants of equine infectious anemia virus during persistent infection. J. Virol. **57:**71–80.
34. **Schoonman, M. J., R. M. Knegtel, and P. D. Grootenhuis.** 1998. Practical evaluation of comparative modelling and threading methods. Comput. Chem. **22:**369–375.
35. **Segawa, H., T. Yamashita, M. Kawakita, and H. Taira.** 2000. Functional analysis of the individual oligosaccharide chains of Sendai virus fusion protein. J. Biochem. (Tokyo) **128:**65–72.
36. **Si, Z., N. Madani, J. M. Cox, J. J. Chruma, J. C. Klein, A. Schon, N. Phan, L. Wang, A. C. Biorn, S. Cocklin, I. Chaiken, E. Freire, A. B. Smith III, and J. G. Sodroski.** 2004. Small-molecule inhibitors of HIV-1 entry block receptor-induced conformational changes in the viral envelope glycoproteins. Proc. Natl. Acad. Sci. USA **101:**5036–5041.
37. **Skehel, J. J., D. J. Stevens, R. S. Daniels, A. R. Douglas, M. Knossow, I. A. Wilson, and D. C. Wiley.** 1984. A carbohydrate side chain on hemagglutinins of Hong Kong influenza viruses inhibits recognition by a monoclonal antibody. Proc. Natl. Acad. Sci. USA **81:**1779–1783.
38. **Takimoto, T., G. L. Taylor, H. C. Connaris, S. J. Crennell, and A. Portner.** 2002. Role of the hemagglutinin-neuraminidase protein in the mechanism of paramyxovirus-cell membrane fusion. J. Virol. **76:**13028–13033.
39. **Tan, C. T., and K. T. Wong.** 2003. Nipah encephalitis outbreak in Malaysia. Ann. Acad. Med. Singapore **32:**112–117.
40. **von Messling, V., and R. Cattaneo.** 2003. N-linked glycans with similar location in the fusion protein head modulate paramyxovirus fusion. J. Virol. **77:**10202–10212.
41. **Wang, L.-F., M. Yu, E. Hansson, L. I. Pritchard, B. Shiell, W. P. Michalski, and B. T. Eaton.** 2000. The exceptionally large genome of Hendra virus: support for creation of a new genus within the family *Paramyxoviridae*. J. Virol. **74:**9972–9979.
42. **Wei, X., J. M. Decker, S. Wang, H. Hui, J. C. Kappes, X. Wu, J. F. Salazar-Gonzalez, M. G. Salazar, J. M. Kilby, M. S. Saag, N. L. Komarova, M. A. Nowak, B. H. Hahn, P. D. Kwong, and G. M. Shaw.** 2003. Antibody neutralization and escape by HIV-1. Nature **422:**307–312.
43. **Wild, C. T., D. C. Shugars, T. K. Greenwell, C. B. McDanal, and T. J. Matthews.** 1994. Peptides corresponding to a predictive alpha-helical domain of human immunodeficiency virus type 1 gp41 are potent inhibitors of virus infection. Proc. Natl. Acad. Sci. USA **91:**9770–9774.
44. **Wildlife Trust.** 28 April 2004, posting date. Nipah virus breaks out in Bangladesh: mortality rates of 60% to 74%. Human to-human transmission may be implicated. Wildlife Trust, New York, N.Y. [Online.] www.ewire.com/display.cfm/Wire_ID/2117.
45. **Wong, K. T., W. J. Shieh, S. Kumar, K. Norain, W. Abdullah, J. Guarner, C. S. Goldsmith, K. B. Chua, S. K. Lam, C. T. Tan, K. J. Goh, H. T. Chong, R. Jusoh, P. E. Rollin, T. G. Ksiazek, and S. R. Zaki.** 2002. Nipah virus infection: pathology and pathogenesis of an emerging paramyxoviral zoonosis. Am. J. Pathol. **161:**2153–2167.
46. **World Health Organization.** 2004. Nipah virus outbreak(s) in Bangladesh, January-April 2004. Wkly. Epidemiol. Rec **79:**168–171.
47. **Yao, Q., and R. W. Compans.** 1996. Peptides corresponding to the heptad repeat sequence of human parainfluenza virus fusion protein are potent inhibitors of virus infection. Virology **223:**103–112.
48. **Yin, H. S., R. G. Paterson, X. Wen, R. A. Lamb, and T. S. Jardetzky.** 2005. Structure of the uncleaved ectodomain of the paramyxovirus (hPIV3) fusion protein. Proc. Natl. Acad. Sci. USA **102:**9288–9293.
49. **Zaitsev, V., M. von Itzstein, D. Groves, M. Kiefel, T. Takimoto, A. Portner, and G. Taylor.** 2004. Second sialic acid binding site in Newcastle disease virus hemagglutinin-neuraminidase: implications for fusion. J. Virol. **78:**3733–3741.